WILEY-VCH

RESEARCH ARTICLE OPEN ACCESS

Non-Minimal Modeling and Structure-Preserving Integration for Planar Elastically Coupled Systems

Paul Kotyczka[1] 🆔 | Anja Götz[2] | Maximilian Herrmann[1]

[1]Department of Engineering Physics and Computation, TUM School of Engineering and Design, Munich Institute of Robotics and Machine Intelligence (MIRMI), Technical University of Munich, Garching, Germany | [2]German Aerospace Center (DLR), Institute of Robotics and Mechatronics, Weßling, Germany

Correspondence: Paul Kotyczka (kotyczka@tum.de)

ABSTRACT

A generalized formulation of evolution equations, which contains gradient and Hamiltonian systems, has been recently discussed in the context of systematic energy-preserving spatial discretization and time integration using a Galerkin and Petrov–Galerkin ansatz, respectively. Among the examples from different physical domains, mechanical systems with holonomic constraints, described in terms of non-minimal configuration variables and velocities, fit into the formulation. The models feature only the derived constraints on velocity level, and they can be numerically integrated, preserving energy and constraints without drift-off. In this contribution, we set up this formulation for *N*-link planar manipulators with mono- or multi-articular elastic couplings in redundant Cartesian coordinates and velocities. Before sketching the recursive construction of the model, we recall the variational principle the model is derived from. A three-link configuration is used as a simulation example to display the numerical conservation of constraints and energy. Finally, we discuss the extension of the model by joint torque inputs and perspectives regarding control design.

1 | Introduction

The dynamics of classical robotic manipulators, for example, rigid industrial robots with revolute joints, are typically written in the second-order form

$$\boldsymbol{M}(\boldsymbol{q})\ddot{\boldsymbol{q}} + \boldsymbol{C}(\boldsymbol{q},\dot{\boldsymbol{q}})\dot{\boldsymbol{q}} + \nabla V(\boldsymbol{q}) = \boldsymbol{\tau} + \boldsymbol{\tau}_{\text{ext}}, \quad (1)$$

where the joint angles $\boldsymbol{q} \in \mathbb{R}^N$ are the *minimal* configuration variables (coordinates), and $\dot{\boldsymbol{q}}, \ddot{\boldsymbol{q}} \in \mathbb{R}^N$ are the joint velocities and accelerations, respectively [1]. $\boldsymbol{\tau} \in \mathbb{R}^N$ denotes the vector of joint torques, and we consider here no external torques, $\boldsymbol{\tau}_{\text{ext}} = \boldsymbol{0}$. Mass and Coriolis matrices $\boldsymbol{M}(\boldsymbol{q})$ and $\boldsymbol{C}(\boldsymbol{q},\dot{\boldsymbol{q}})$ (with $\boldsymbol{M}(\boldsymbol{q})$ symmetric and positive definite and $\dot{\boldsymbol{M}}(\boldsymbol{q}) - 2\boldsymbol{C}(\boldsymbol{q},\dot{\boldsymbol{q}})$ skew-symmetric), as well as the gradient of the potential energy $\nabla V(\boldsymbol{q})$, depend in such

a formulation highly on combined trigonometric functions of the joint angles.

Non-minimal or *redundant* coordinates are used in *global* formulations [2], which come without local parameterizations like joint angles. Such formulations take into account the topology of the configuration space, for example, the *special orthogonal group* SO(3) for rigid body rotations [3] or $(S^1)^N$ for serial manipulators [4], and are singularity-free. Typically, *minimal* velocity coordinates are used, for example, the relative joint angular velocities, which then are related to the absolute translational and angular velocities of the bodies via the *manipulator Jacobian*. The evolution of non-minimal coordinates is subject to *holonomic constraints*, that is, constraints on configuration level. In numerical integration, these can be satisfied by either ensuring the confinement to the configuration manifold via

a suitable retraction map, as is done in *Lie group variational integrators* [5], or, without pronouncing the geometric perspective, via satisfaction of the algebraic constraint equations and/or their derivatives.

In [6], the conservation of energy and total angular momentum, as well as the fulfillment of constraints on configuration and velocity level, are shown with a family of *mixed Galerkin* schemes and illustrated with simulations of rigid-body and coupled rigid-flexible systems. In [7], a generalized gradient/Hamiltonian form of evolution equations is the foundation for energy-preserving spatial discretization with *Galerkin* and numerical integration with *Petrov–Galerkin* schemes. Mechanical systems with derived holonomic constraints fit in the considered equation structure, and simulations with a planar pendulum exemplify constraint and energy preservation with non-minimal Cartesian coordinates and velocities. The corresponding formulation, according to [7], augmented by the action of joint torque inputs, has the structure

$$
\begin{bmatrix}
\mathbf{0} & \mathbf{M} & -\mathbf{G}^\top(\mathbf{x}) \\
-\mathbf{M} & \mathbf{0} & \mathbf{0} \\
\mathbf{G}(\mathbf{x}) & \mathbf{0} & \mathbf{0}
\end{bmatrix}
\begin{bmatrix}
\dot{\mathbf{x}} \\
\ddot{\mathbf{x}} \\
\dot{\mathbf{\Lambda}}
\end{bmatrix}
= -
\begin{bmatrix}
\nabla_x H(\mathbf{x}, \dot{\mathbf{x}}) \\
\nabla_{\dot{x}} H(\mathbf{x}, \dot{\mathbf{x}}) \\
\mathbf{0}
\end{bmatrix}
+
\begin{bmatrix}
\mathbf{B}(\mathbf{x}) \\
\mathbf{0} \\
\mathbf{0}
\end{bmatrix}
\tau,
$$

(2)

where $\mathbf{x}, \dot{\mathbf{x}} \in \mathbb{R}^n$ are the absolute Cartesian positions and velocities, and $\mathbf{\Lambda} \in \mathbb{R}^m$ denotes the vector of *integrated* Lagrange multipliers. A characteristic feature of using absolute Cartesian coordinates and velocities is the *constant mass matrix* in the formulation of the Hamiltonian, $H(\mathbf{x}, \dot{\mathbf{x}}) = \frac{1}{2}\dot{\mathbf{x}}^\top \mathbf{M} \dot{\mathbf{x}} + V(\mathbf{x})$.

Using non-minimal, redundant, or *natural* coordinates for multibody modeling and simulation [8, 9] or optimal control [10] is a well-developed idea, including their efficient structure-preserving numerical schemes [11]. The focus of this contribution is to present the modeling in the form of (2) of a *planar N*-link serial mechanism with *mono- or multi-articular elastic couplings*, accompanied with simulation results displaying the properties of (exact and approximate) energy-preserving integration. Providing a rigid-body robotic structure with elastic components like tendons or artificial muscles in a typically antagonistic form, as sketched in Figure 1, mimics the musculoskeletal system of human or animal extremities and can allow for highly efficient, for example, repetitive, motions.

In Section 2, we recall the variational derivation of the model structure (2) and its energy-preserving integration according to [7]. The considered elastically coupled *N*-link serial kinematics are introduced in Section 3, and the expressions for energies and (differentiated) constraints are derived in terms of Cartesian coordinates and velocities. Section 4 shows simulation results using the lowest order Petrov–Galerkin scheme and its midpoint approximation, which illustrate the need for (sufficiently) exact quadrature of non-polynomial energy gradients. In Section 5, the structural relation between derived constraint and joint input matrices is exploited to relate the Cartesian modeling to the absolute description of the configuration in terms of rotation matrices of elements of SO(2). The formulation of a classical impedance control law in terms of only Cartesian link coordinates and TCP coordinates follows immediately. Section 6 gives concluding remarks and points to current research activities.
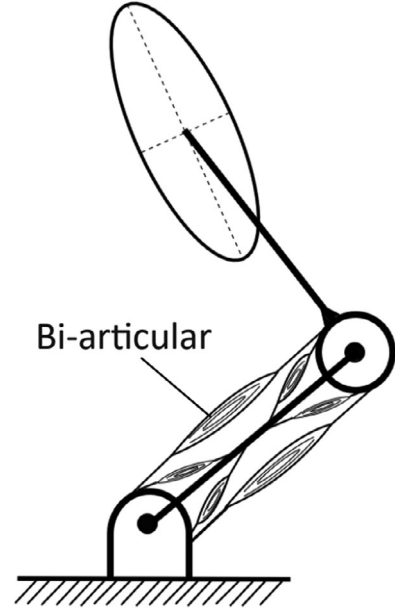

FIGURE 1 | Sketch of a planar two-link mechanism, consisting of rigid links with mono- and bi-articular elastic coupling. The stiffness ellipsoid is indicated at the TCP (with kind permission of Hannes Höppner).

2 | Constrained Mechanical Systems

We briefly summarize the formulation of constrained mechanical systems in the generalized gradient form, which can be integrated in an energy- and constraint-preserving way using *Petrov–Galerkin* schemes [7]. Such integration methods had already been proposed as a family of *mixed Galerkin* time finite element schemes in [6] for an augmented formulation [12], which contains both the constraints on coordinate and velocity level (4) and (9).

2.1 | Generalized Gradient Formulation

We consider mechanical multibody systems, in a first step without external forces and torques, written in absolute Cartesian positions $\mathbf{x}$ and velocities $\dot{\mathbf{x}}$ of their centers of gravity (COGs), with Lagrangian

$$
L(\mathbf{x}, \dot{\mathbf{x}}) = \frac{1}{2}\dot{\mathbf{x}}^\top \mathbf{M} \dot{\mathbf{x}} - V(\mathbf{x}).
$$

(3)

Due to this choice of non-minimal coordinates and velocities, the mass matrix $\mathbf{M} = \mathbf{M}^\top > 0$ is constant, which will be assumed in the sequel.[1] Holonomic constraints are expressed by the set of algebraic equations

$$
\mathbf{g}(\mathbf{x}) = \mathbf{0},
$$

(4)

and the modified Lagrangian[2] reads

$$
\bar{L}(\mathbf{x}, \dot{\mathbf{x}}, \boldsymbol{\lambda}) = L(\mathbf{x}, \dot{\mathbf{x}}) + \mathbf{g}^\top(\mathbf{x})\boldsymbol{\lambda}.
$$

(5)

The stationarity condition according to Hamilton's principle

$$\delta \int_0^T \bar{L}(\boldsymbol{x}, \dot{\boldsymbol{x}}, \boldsymbol{\lambda})\, dt = \int_0^T \frac{\partial \bar{L}}{\partial \boldsymbol{x}}\delta \boldsymbol{x} + \frac{\partial \bar{L}}{\partial \dot{\boldsymbol{x}}}\delta \dot{\boldsymbol{x}} + \frac{\partial \bar{L}}{\partial \boldsymbol{\lambda}}\delta \boldsymbol{\lambda}\, dt = 0 \quad (6)$$

becomes, after integration by parts and introducing the integrated Lagrange multipliers, $\boldsymbol{\Lambda}(t) = \boldsymbol{\Lambda}(0) + \int_0^t \boldsymbol{\lambda}(\tau)\, d\tau$,

$$\int_0^T \left(\frac{\partial \bar{L}}{\partial \boldsymbol{x}} - \frac{d}{dt}\frac{\partial \bar{L}}{\partial \dot{\boldsymbol{x}}} \right)\delta \boldsymbol{x} - \frac{d}{dt}\frac{\partial \bar{L}}{\partial \boldsymbol{\lambda}}\delta \boldsymbol{\Lambda}\, dt + \left[\frac{\partial \bar{L}}{\partial \dot{\boldsymbol{x}}}\delta \boldsymbol{x} + \frac{\partial \bar{L}}{\partial \boldsymbol{\lambda}}\delta \boldsymbol{\Lambda} \right]_0^T = 0. \quad (7)$$

The boundary term vanishes due to $\delta \boldsymbol{x}(0) = \delta \boldsymbol{x}(T) = \boldsymbol{0}$ and $\frac{\partial \bar{L}}{\partial \boldsymbol{\lambda}} = \boldsymbol{g}^\top(\boldsymbol{x}) = \boldsymbol{0}^\top$. Satisfaction of (7) for all $\delta \boldsymbol{x}$ and $\delta \boldsymbol{\Lambda}$ leads to the Euler–Lagrange equations

$$\frac{d}{dt}\left(\frac{\partial \bar{L}}{\partial \dot{\boldsymbol{x}}} \right)^\top - \left(\frac{\partial \bar{L}}{\partial \boldsymbol{x}} \right)^\top = \boldsymbol{M}\ddot{\boldsymbol{x}} - \boldsymbol{G}^\top(\boldsymbol{x})\boldsymbol{\lambda} + \nabla V(\boldsymbol{x}) = \boldsymbol{0} \quad (8)$$

and the constraint equations on velocity level,

$$\frac{d}{dt}\left(\frac{\partial \bar{L}}{\partial \boldsymbol{\lambda}} \right)^\top = \boldsymbol{G}(\boldsymbol{x})\dot{\boldsymbol{x}} = \boldsymbol{0}, \quad (9)$$

with the derived constraint matrix

$$\boldsymbol{G}(\boldsymbol{x}) = \frac{\partial \boldsymbol{g}(\boldsymbol{x})}{\partial \boldsymbol{x}}. \quad (10)$$

Writing the Hamiltonian, which is the sum of kinetic and potential energy

$$H(\boldsymbol{x}, \dot{\boldsymbol{x}}) = \frac{1}{2}\dot{\boldsymbol{x}}^\top \boldsymbol{M}\dot{\boldsymbol{x}} + V(\boldsymbol{x}), \quad (11)$$

in terms of coordinates and velocities instead of momenta,[3] Equations (8) and (9) can be combined, together with the kinematic equation $\boldsymbol{M}\dot{\boldsymbol{x}} = \nabla_{\dot{\boldsymbol{x}}}H$, to obtain the generalized gradient formulation (2).

If the initial value lies on the constraint manifold, $\boldsymbol{g}(\boldsymbol{x}(0)) = \boldsymbol{0}$, the constraints are preserved according to the third line of (2). Multiplying both sides from the left with $\begin{bmatrix} \dot{\boldsymbol{x}}^\top & \ddot{\boldsymbol{x}}^\top & \dot{\boldsymbol{\Lambda}}^\top \end{bmatrix}$ leads to $\dot{H}(\boldsymbol{x}, \dot{\boldsymbol{x}}) = \boldsymbol{0}$ by skew-symmetry of the left-hand matrix and the application of the chain rule on the right.

The input matrix $\boldsymbol{B}(\boldsymbol{x})$, through which joint torques $\boldsymbol{\tau} \in \mathbb{R}^N$ enter the equations of motion, will be derived in Subsection 3.5 for the considered case of planar serial manipulators.

2.2 | Energy- and Constraint-Preserving Integration

Equation (2) is a representative of a system in a generalized gradient or Hamiltonian structure.[4] We adopt here the notation from [7] with $\boldsymbol{u} \in V = \mathbb{R}^d$ the vector of unknowns and $\partial_t \boldsymbol{u}$ its time derivative,

$$\boldsymbol{C}(\boldsymbol{u})\partial_t \boldsymbol{u} = -\nabla H(\boldsymbol{u}), \quad \text{where} \quad \boldsymbol{C}(\boldsymbol{u}) = -\boldsymbol{C}^\top(\boldsymbol{u}). \quad (12)$$

The formulation (2) fits into this frame with $\boldsymbol{u}^\top = \begin{bmatrix} \boldsymbol{x}^\top & \dot{\boldsymbol{x}}^\top & \boldsymbol{\Lambda}^\top \end{bmatrix}$ and $\nabla_\Lambda H(\boldsymbol{u}) = \boldsymbol{0}$. With $\boldsymbol{u}$ the vector of trial functions, a weak formulation is

$$(\boldsymbol{C}(\boldsymbol{u})\partial_t \boldsymbol{u}, \boldsymbol{v})_I = -(\nabla H(\boldsymbol{u}), \boldsymbol{v})_I \quad (13)$$

for all suitable test functions $\boldsymbol{v} \in V$ and the L^2 inner product $(\boldsymbol{a}, \boldsymbol{b})_I = \int_I \boldsymbol{a} \cdot \boldsymbol{b}\, dt$ on an arbitrary time interval $I = [0, T]$. Energy conservation follows immediately from skew-symmetry of $\boldsymbol{C}(\boldsymbol{u})$ when testing with $\boldsymbol{v} = \partial_t \boldsymbol{u}$:

$$\underbrace{(\boldsymbol{C}(\boldsymbol{u})\partial_t \boldsymbol{u}, \partial_t \boldsymbol{u})_I}_{=0} = -\underbrace{(\nabla H(\boldsymbol{u}), \partial_t \boldsymbol{u})_I}_{=H(T)-H(0)}. \quad (14)$$

A Petrov–Galerkin (or mixed Galerkin) discretization of (13) consists in subdividing I in (here equidistant) intervals $I_k = [t_k, t_{k+1}]$ over a time grid $T_N = \{t_0, t_1, \ldots, t_N\}$ such that $I = \cup_{k=1}^N I_k$. The approximate solution of (13) is sought

- in the finite-dimensional subspace of trial functions $\boldsymbol{u}_h \in P_{m+1}(T_N; V) \cap H^1(I; V)$

- for all test functions $\boldsymbol{v}_h \in P_m(T_N; V)$.

$P_m(T_N; V) \cap H^1(I; V)$ denotes the space of V-valued piecewise polynomial and weakly differentiable functions, such that also on the discrete level the energy balance equation is satisfied,

$$\underbrace{(\boldsymbol{C}(\boldsymbol{u}_h)\partial_t \boldsymbol{u}_h, \partial_t \boldsymbol{u}_h)_{I_k}}_{=0} = -\underbrace{(\nabla H(\boldsymbol{u}_h), \partial_t \boldsymbol{u}_h)_{I_k}}_{=H(t_{k+1})-H(t_k)}, \quad (15)$$

as long as the integral on the right hand side can be evaluated *exactly* (or with sufficient precision).

The exact conservation of constraints without drift-off for mechanical systems of the form (2) can be shown using piecewise constant test functions, see [7], Remark 8.

2.3 | Lowest Order Petrov–Galerkin Integration and Midpoint Rule

For $m = 0$, the trial functions are piecewise linear and continuous at the interval boundaries,

$$\boldsymbol{u}_h(t) = \boldsymbol{u}_k + \frac{\boldsymbol{u}_{k+1} - \boldsymbol{u}_k}{h}(t - t_k) \quad \text{on } I_k. \quad (16)$$

Accordingly, the time derivatives are piecewise constant,

$$\partial_t \boldsymbol{u}_h(t) = \frac{\boldsymbol{u}_{k+1} - \boldsymbol{u}_k}{h} \quad \text{on } I_k. \quad (17)$$

Substituting $\boldsymbol{u}_h(t)$ and $\partial_t \boldsymbol{u}_h(t)$ in the weak formulation (13), and testing with piecewise constant test functions $\boldsymbol{v}_h = const.$ on I_k (which can be canceled on both sides) gives

$$\int_{t_k}^{t_{k+1}} \boldsymbol{C}(\boldsymbol{u}_h(t))\, dt\, \frac{\boldsymbol{u}_{k+1} - \boldsymbol{u}_k}{h} = -\int_{t_k}^{t_{k+1}} \nabla H(\boldsymbol{u}_h(t))\, dt. \quad (18)$$

If the elements of $\boldsymbol{C}(\boldsymbol{u})$ are at most linear in $\boldsymbol{u}$—which will be the case for the considered class of systems—the left-hand integral

TABLE 1 | Declaration of coordinates and angles.

Symbol	Description
$\boldsymbol{X}_i = (X_i, Y_i)$	i-th revolute joint coordinate w.r.t. the inertial frame
$\boldsymbol{x}_i = (x_i, y_i)$	i-th link's center of gravity w.r.t. the inertial frame
$\boldsymbol{\xi}_i = (\xi_i, \eta_i)$	i-th link's center of gravity w.r.t. the joint frame
φ_i	i-th joint angle (relative)
ϕ_i	i-th joint angle (absolute)

TABLE 2 | Simple parameters for the simulation examples.

	Symbol	Value	Unit
Mass	m_i	1	kg
Moment of inertia	J_i	1	kg m^2
Link length	L_i	1	1
Link COG distance	l_i	0.5	m
Spring fastening distance	r_i	0.4	m
Relaxed spring length	$s_{i,0}$	0.2	m
Spring stiffness	k_i	1	N/m
Gravitational acceleration	g	1	m/s^2
Initial values	$\boldsymbol{\xi}_i(0)$	$(l_i, 0)$	m

Note: Identical parameters for each link, $i = 1, 2, 3$.

is exactly integrated with one-stage Gauss quadrature, and the integration scheme can be written in the implicit form

$$C \left(\frac{\boldsymbol{u}_k + \boldsymbol{u}_{k+1}}{2} \right)(\boldsymbol{u}_{k+1} - \boldsymbol{u}_k) = -\int_{t_k}^{t_{k+1}} \nabla H(\boldsymbol{u}_h(t))\, dt. \quad (19)$$

If also the gradient of the Hamiltonian is linear, the energy-conserving scheme boils down to an implicit midpoint rule

$$C \left(\frac{\boldsymbol{u}_k + \boldsymbol{u}_{k+1}}{2} \right)(\boldsymbol{u}_{k+1} - \boldsymbol{u}_k) = -h \nabla H \left(\frac{\boldsymbol{u}_k + \boldsymbol{u}_{k+1}}{2} \right). \quad (20)$$

Otherwise, the right-hand side of (19) must be evaluated with a sufficiently accurate quadrature rule Table 1.

3 | Elastically Coupled Planar Serial Manipulators

We describe the modeling of an N-link serial manipulator in terms of redundant coordinates and velocities, see Figure 2 for a sketch with $N = 2$. We follow a "direct" approach, and the coordinates and velocities of the i-th center of gravity (COG)

$$\boldsymbol{\xi}_i = (\xi_i, \eta_i) \qquad \text{and} \qquad \dot{\boldsymbol{\xi}}_i = (\dot{\xi}_i, \dot{\eta}_i) \quad (21)$$

are defined relative to the respective coordinate system in the i-th joint, which is aligned with the inertial frame. In Table 2, all absolute and relative Cartesian coordinates and joint angles are declared. $\boldsymbol{\xi}_i \in \mathbb{R}^2$ and $\dot{\boldsymbol{\xi}}_i \in \mathbb{R}^2$ replace the roles of minimal joint coordinates and velocities. For a complete and systematic exposition of robot kinematics and dynamics, see for example, [1].
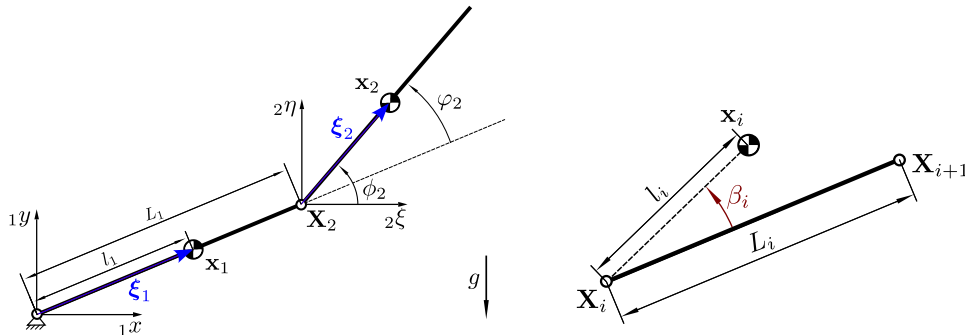
3.1 | Kinematics

We consider the case depicted on the left of Figure 2, where each link's (length L_i) center of gravity (COG) lies on the centerline between the joints at distance l_i.[5] The joint and the COG coordinates can then recursively be determined from

$$\boldsymbol{x}_i = \boldsymbol{X}_i + \boldsymbol{\xi}_i, \qquad \boldsymbol{X}_{i+1} = \boldsymbol{X}_i + \alpha_i \boldsymbol{\xi}_i, \qquad \alpha_i = \frac{L_i}{l_i}.$$

Starting from $\boldsymbol{X}_1 = \boldsymbol{0}$, absolute COG coordinates $\boldsymbol{x}_i$ can be computed from the relative Cartesian joint coordinates $\boldsymbol{\xi}_i$ recursively. The forward kinematics is given by a lower-triangular linear coordinate transformation

$$\boldsymbol{x} = \boldsymbol{J}\boldsymbol{\xi} \qquad \text{with} \qquad \boldsymbol{J} = \begin{bmatrix} 1 & & & \\ \alpha_1 & 1 & & \\ \alpha_1 & \alpha_2 & 1 & \\ \vdots & \vdots & \ddots & \ddots \end{bmatrix} \otimes \boldsymbol{I}_2, \quad (22)$$

where $\otimes$ denotes the Kronecker product and $\boldsymbol{I}_2$ is the identity matrix. The same transformation holds on velocity level, $\dot{\boldsymbol{x}} = \boldsymbol{J}\dot{\boldsymbol{\xi}}$, so $\boldsymbol{J} \in \mathbb{R}^{2N \times 2N}$ plays the role of the spatial system Jacobian [13]. The forward kinematics mapping for the tool center point (TCP) and the according Jacobian are clearly given by

$$\boldsymbol{x}_{\text{tcp}} = \boldsymbol{J}_{\text{tcp}}\boldsymbol{\xi}, \qquad \dot{\boldsymbol{x}}_{\text{tcp}} = \boldsymbol{J}_{\text{tcp}}\dot{\boldsymbol{\xi}} \qquad \text{with}$$

$$\boldsymbol{J}_{\text{tcp}} = \begin{bmatrix} \alpha_1 & \cdots & \alpha_N \end{bmatrix} \otimes \boldsymbol{I}_2. \quad (23)$$

FIGURE 2 | Coordinates of centers of gravity (COG) and joints in a two-link example (left). Detail on considering an eccentric COG (right).

By the use of non-minimal velocities, the unique inverse transformation (inverse spatial Jacobian) exists and is given by

$$\dot{\boldsymbol{\xi}} = \boldsymbol{J}^{-1}\dot{\boldsymbol{x}} \qquad \text{with} \qquad \boldsymbol{J}^{-1} = \begin{bmatrix} \boldsymbol{t}_1^\top \\ \vdots \\ \boldsymbol{t}_N^\top \end{bmatrix} \otimes \boldsymbol{I}_2. \qquad (24)$$

The row vectors $\boldsymbol{t}_i^\top$, which will be required further below, take the forms[6]

$$\boldsymbol{t}_i^\top = \begin{bmatrix} -\alpha_1 \prod_{j=2}^{i-1}(1-\alpha_j) & \cdots & -\alpha_{i-2}(1-\alpha_{i-1}) & \alpha_{i-1} & 1 & 0 & \cdots & 0 \end{bmatrix}. \qquad (25)$$

The vectors of relative joint angles $\boldsymbol{\varphi} \in \mathbb{R}^N$ and absolute joint angles $\boldsymbol{\phi} \in \mathbb{R}^N$ are related via

$$\boldsymbol{\varphi} = \boldsymbol{D}\boldsymbol{\phi} \qquad \text{with} \qquad \boldsymbol{D} = \begin{bmatrix} 1 & & & \\ -1 & 1 & & \\ & \ddots & \ddots & \\ & & -1 & 1 \end{bmatrix} \quad \Leftrightarrow$$

$$\boldsymbol{D}^{-1} = \begin{bmatrix} 1 & & & \\ 1 & 1 & & \\ 1 & 1 & 1 & \\ \vdots & \vdots & \vdots & \ddots \end{bmatrix}. \qquad (26)$$

3.2 | Constraints and Relations to Joint Velocities

The relative Cartesian positions $\boldsymbol{\xi}_i$ of the COGs are constrained by

$$g_i = \frac{1}{2}\boldsymbol{\xi}_i^\top \boldsymbol{\xi}_i - \frac{1}{2}l_i^2 = 0. \qquad (27)$$

Summarizing the time derivatives

$$\dot{g}_i = \boldsymbol{\xi}_i^\top \dot{\boldsymbol{\xi}} = \boldsymbol{\xi}_i^\top \boldsymbol{J}^{-1}\dot{\boldsymbol{x}} = (\boldsymbol{t}_i^\top \otimes \boldsymbol{\xi}_i^\top)\dot{\boldsymbol{x}} = 0 \qquad (28)$$

in $\dot{\boldsymbol{g}} = \boldsymbol{G}(\boldsymbol{\xi})\dot{\boldsymbol{x}} = \boldsymbol{0}$, we obtain the matrix $\boldsymbol{G}(\boldsymbol{\xi}) \in \mathbb{R}^{N \times 2N}$, describing the derived constraints. Substituting $\boldsymbol{\xi} = \boldsymbol{J}^{-1}\boldsymbol{x}$ immediately gives the formulation $\boldsymbol{G}(\boldsymbol{x})$ in absolute Cartesian coordinates[7]

$$\boldsymbol{G}(\boldsymbol{\xi}) = \begin{bmatrix} \boldsymbol{t}_1^\top \otimes \boldsymbol{\xi}_1^\top \\ \vdots \\ \boldsymbol{t}_N^\top \otimes \boldsymbol{\xi}_N^\top \end{bmatrix}. \qquad (29)$$

The relations between the vectors of relative Cartesian velocities $\dot{\boldsymbol{\xi}}_i$ and the absolute joint angular velocities $\dot{\phi}_i$ are

$$l_i^2 \dot{\phi}_i^{\;2} = \dot{\boldsymbol{\xi}}_i^\top \dot{\boldsymbol{\xi}}_i, \qquad (30a)$$

$$l_i^2 \dot{\phi}_i = (\boldsymbol{\xi}_i^\perp)^\top \dot{\boldsymbol{\xi}}_i \qquad \Leftrightarrow \qquad \dot{\boldsymbol{\xi}}_i = \boldsymbol{\xi}_i^\perp \dot{\phi}_i, \qquad (30b)$$

where $\boldsymbol{\xi}_i^\perp = (-\eta_i, \xi_i)$ results from $\boldsymbol{\xi}_i$ through rotation by 90°:

$$\boldsymbol{\xi}_i^\perp = \begin{bmatrix} 0 & -1 \\ 1 & 0 \end{bmatrix} \boldsymbol{\xi}_i = \boldsymbol{R}\left(\frac{\pi}{2}\right)\boldsymbol{\xi}_i. \qquad (31)$$
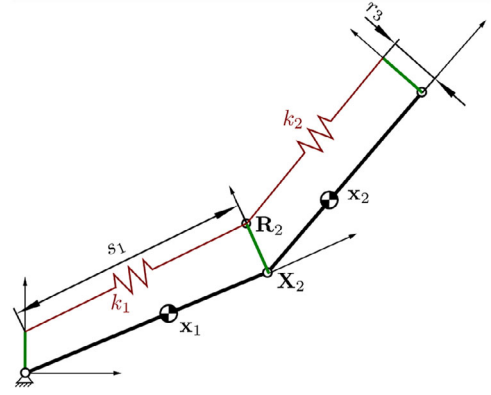

FIGURE 3 | Simple realization of cross-link elastic couplings in a planar two-link example.

Vector versions of (30b) are

$$\boldsymbol{L}^2\dot{\boldsymbol{\phi}} = \text{diag}\{(\boldsymbol{\xi}_1^\perp)^\top, \ldots, (\boldsymbol{\xi}_N^\perp)^\top\}\dot{\boldsymbol{\xi}} \qquad \text{and} \qquad \dot{\boldsymbol{\xi}} = \text{diag}\{\boldsymbol{\xi}_1^\perp, \ldots, \boldsymbol{\xi}_N^\perp\}\dot{\boldsymbol{\phi}} \qquad (32)$$

with $\boldsymbol{L} = \text{diag}\{l_1, \ldots, l_N\}$ and the Jacobian $\frac{\partial \boldsymbol{\xi}}{\partial \boldsymbol{\phi}} = \text{diag}\{\boldsymbol{\xi}_1^\perp, \ldots, \boldsymbol{\xi}_N^\perp\}$.

3.3 | Kinetic and Potential Energies

Using (30a) and (24), we can express the kinetic energy

$$T(\dot{\boldsymbol{x}}, \dot{\boldsymbol{\phi}}) = \sum_{i=1}^{N} \frac{1}{2}m_i\dot{x}_i^2 + \frac{1}{2}m_i\dot{y}_i^2 + \frac{1}{2}J_i\dot{\phi}_i^2, \qquad (33)$$

where m_i and J_i are masses of the links and their moments of inertia around the COG, purely in terms of the Cartesian velocities and a constant mass matrix:

$$T(\dot{\boldsymbol{x}}) = \frac{1}{2}\dot{\boldsymbol{x}}^\top \boldsymbol{M}\dot{\boldsymbol{x}} \qquad \text{with}$$

$$\boldsymbol{M} = \left(\text{diag}\{m_1, \ldots, m_N\} + \sum_{i=1}^{N} \frac{J_i}{l_i^2}\boldsymbol{t}_i\boldsymbol{t}_i^\top\right) \otimes \boldsymbol{I}_2. \qquad (34)$$

The potential energy due to gravity is simply

$$V_g(\boldsymbol{x}) = \sum_{i=1}^{N} m_i g y_i. \qquad (35)$$

3.4 | Elastic Potentials

For the inclusion of elastic couplings between links, consider Figure 3 for a simple, exemplary setting. Springs (as finite-dimensional abstractions of elastic tendons with stiffness k_i each) are guided in parallel to the links, attached at an angle of 90° at the ends of the links. The length of the i-th spring is the Euclidean norm of the vector chain depicted in[8] Figure 4,

$$s_i(\boldsymbol{x}_{i-1}, \boldsymbol{x}_i) = \|\Delta\boldsymbol{X}_i + \boldsymbol{r}_{i+1} - \boldsymbol{r}_i\| \qquad (36)$$
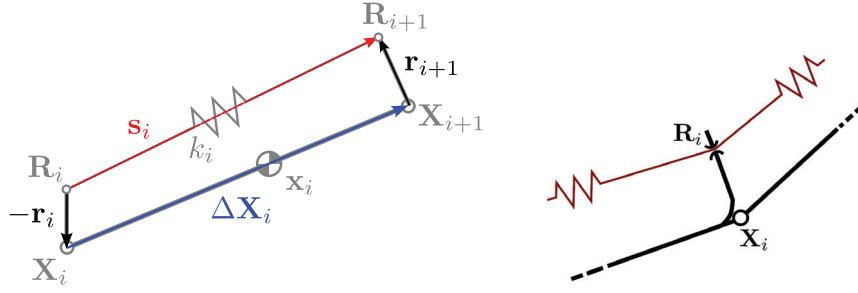
FIGURE 4 | Vector chain to determine the length $s_i = \|\boldsymbol{s}_i\|$ of a single spring (left). Details on the guidance of the spring in the case of multi-articular coupling (right).

with

$$
\boldsymbol{r}_1 = r_1 \begin{bmatrix} 0 \\ 1 \end{bmatrix}, \qquad \Delta\boldsymbol{X}_i = \boldsymbol{X}_{i+1} - \boldsymbol{X}_i, \qquad \boldsymbol{r}_{i+1} = \frac{r_{i+1}}{L_i} \begin{bmatrix} 0 & 1 \\ -1 & 0 \end{bmatrix} \Delta\boldsymbol{X}_i.
$$
(37)

We assume that the springs are under tension for all configurations, meaning that the difference between the current and the relaxed length $\Delta s_i = s_i - s_{i,0}$ is greater than zero for all times. Assuming further linear springs, the stored elastic energy takes the forms

$$
V_{s,\text{mono}} = \sum_{i=1}^{N} \frac{1}{2} k_i \Delta s_i^2 \qquad \text{or} \qquad V_{s,\text{mult}} = \frac{1}{2} k \left(\sum_{i=1}^{N} \Delta s_i \right)^2, \quad (38)
$$

depending on whether the springs are fixed between two links (mono-articular coupling) or a chain of springs (tendon) is guided through the fastenings (multi-articular coupling), see Figure 4. Other than the kinetic and potential energies T and V_g, the elastic potential is non-linear and non-quadratic in the link coordinates $\boldsymbol{x}_i$.

3.5 | Joint Inputs

To complete the control model of the elastically coupled kinematics, we need to determine the matrix $\boldsymbol{B}(\boldsymbol{\xi})$, which maps the joint input torques to forces that apply on the COGs. The energy balance in terms of the COG velocities is

$$
\dot{H} = \dot{\boldsymbol{\varphi}}^\top \boldsymbol{\tau} = \dot{\boldsymbol{x}}^\top \left(\frac{\partial \boldsymbol{\varphi}}{\partial \boldsymbol{x}} \right)^\top \boldsymbol{\tau} = \dot{\boldsymbol{x}}^\top \underbrace{\boldsymbol{B}(\boldsymbol{\xi})\boldsymbol{\tau}}_{F_\tau},
$$
(39)

where $\boldsymbol{F}_\tau \in \mathbb{R}^{2N}$ denotes the resulting control forces to the COGs. We obtain $\boldsymbol{B}(\boldsymbol{\xi})$, which transforms the absolute Cartesian link velocities to relative joint velocities, by concatenating the different Jacobians according to (26), (32), and (24):

$$
\begin{aligned}
\boldsymbol{B}^\top(\boldsymbol{\xi}) &= \frac{\partial \boldsymbol{\varphi}}{\partial \boldsymbol{\phi}} \frac{\partial \boldsymbol{\phi}}{\partial \boldsymbol{\xi}} \frac{\partial \boldsymbol{\xi}}{\partial \boldsymbol{x}} \\
&= \boldsymbol{D}\boldsymbol{L}^{-2}\text{diag}\{(\boldsymbol{\xi}_1^\perp)^\top, \ldots, (\boldsymbol{\xi}_N^\perp)^\top\}\boldsymbol{J}^{-1} \\
&= \boldsymbol{D}\boldsymbol{L}^{-2} \underbrace{\begin{bmatrix} \boldsymbol{t}_1^\top \otimes (\boldsymbol{\xi}_1^\perp)^\top \\ \vdots \\ \boldsymbol{t}_N^\top \otimes (\boldsymbol{\xi}_N^\perp)^\top \end{bmatrix}}_{=\boldsymbol{B}_0^\top(\boldsymbol{\xi})}.
\end{aligned}
$$
(40)

The structurally identical matrices $\boldsymbol{G}(\boldsymbol{\xi})$ and $\boldsymbol{B}_0^\top(\boldsymbol{\xi})$, differing in the orthogonal vectors $\boldsymbol{\xi}_i$ and $\boldsymbol{\xi}_i^\perp$, reflect the complementary nature of constraint and actuation forces.

4 | Numerical Examples

We present numerical examples, which illustrate the conservation properties of the simplest Petrov–Galerkin integration scheme ($m = 0$) and its approximation by the midpoint rule. The model problem is the free motion of a serial three-link kinematics without and with mono-articular couplings. The simple model parameters are given in Table 2. All simulations start from a horizontally stretched configuration, corresponding to absolute joint angles $\phi_i = 0$, $i = 1, 2, 3$.

4.1 | Constraint Preservation

In both scenarios, the derived constraints are described by (28), (29), resulting in a left-hand matrix of (2), which consists of constant elements and linear functions and which can be exactly integrated over every time interval I_k. Accordingly, the squared constraint errors

$$
e_{c,i}^2 = \boldsymbol{\xi}_i^\top \boldsymbol{\xi}_i - l_i^2, \qquad i = 1, 2, 3
$$
(41)

remain in the region of machine precision. Figure 5 also displays how the constraint error (defined w.r.t. relative Cartesian link coordinates) propagates through the kinematic chain.

4.2 | Energy Preservation and Order

In the configuration without springs, the kinetic and potential energies (34), (35) are quadratic and linear in velocities and positions. Consequently, the gradient ∇H can also be integrated exactly with the implicit midpoint rule (20). Figure 6 shows the deviations of the total energy from its initial value

$$
\Delta H(t) = H(t) - H(0).
$$
(42)

For the three-link pendulum without springs (left plot), this energy error has the same magnitude as the violation of the squared constraints. Applying the implicit midpoint rule to the
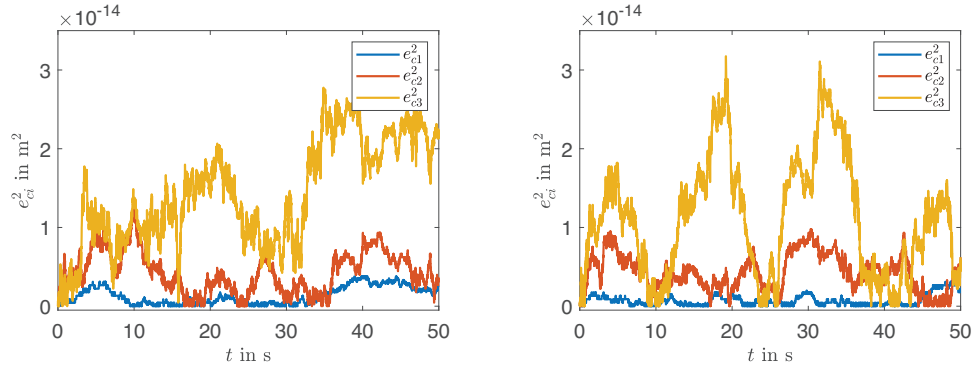
FIGURE 5 | Preservation of the squared constraints under the implicit midpoint rule without springs (left) and with mono-articular couplings (right). Sampling time $h = 0.01$ s.
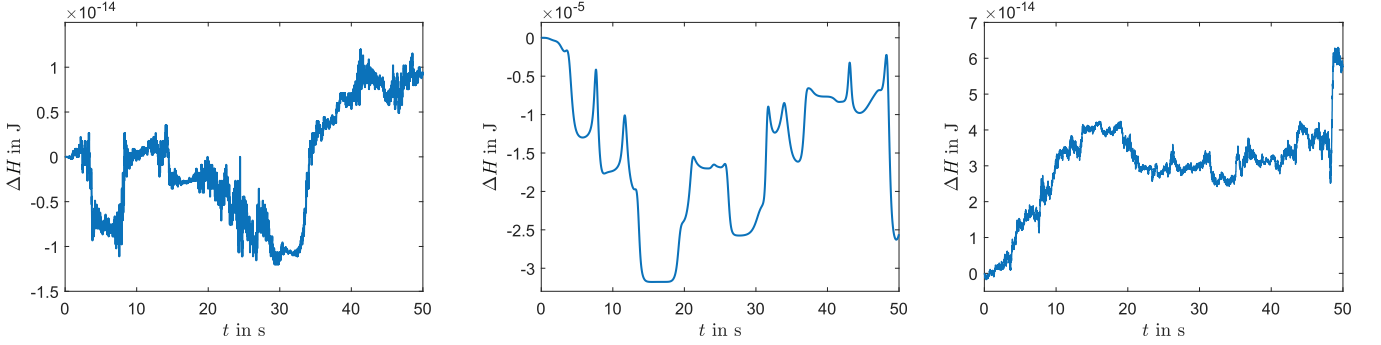

FIGURE 6 | Energy increments without springs under the implicit midpoint rule (left); with mono-articulate couplings under the implicit midpoint rule (middle) and the Petrov–Galerkin scheme using 3-stage Gauss-quadrature to integrate $\nabla V_{s,\text{mono}}(\boldsymbol{x})$ (right). Sampling time $h = 0.01$ s.
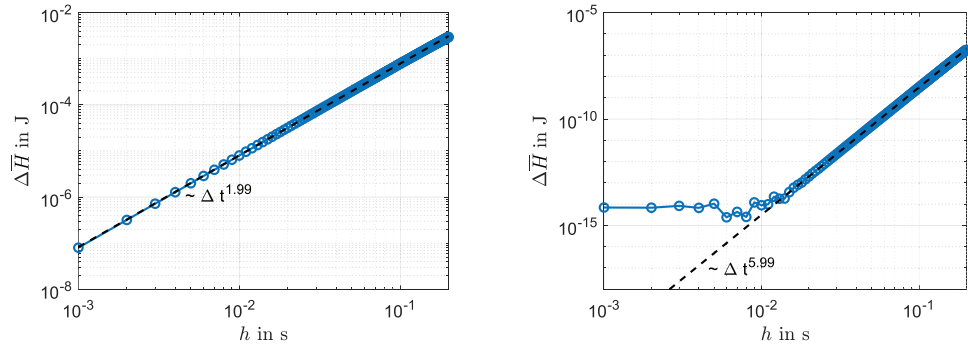

FIGURE 7 | Average energy error over step size for mono-articular couplings under the implicit midpoint rule (left) and the Petrov–Galerkin scheme with 3-stage Gauss-quadrature of $\nabla V_{s,\text{mono}}(\boldsymbol{x})$ (right). Simulation time $T = 10$ s.

model with mono-articular couplings, where the total spring energy is not polynomial, the quadrature error is clearly visible in the magnitude of the energy error ΔH (middle plot). Using 3-point Gauss quadrature to numerically evaluate the integral over ∇H in (19), the energy error is pushed down to machine precision again (right plot).

The two plots in Figure 7 show the average energy error

$$\Delta \bar{H} = \frac{1}{N} \sum_{k=0}^{N} |\Delta H_k| \qquad (43)$$

over different step sizes h for a simulation run of $T = 10$ s for the simulations with mono-articular couplings using the implicit midpoint rule (20) and the Petrov–Galerkin scheme with 3-stage Gauss integration of the right-hand side of (19). The orders 2 and 6 of the numerical approximations of the integral $\int_{t_k}^{t_{k+1}} \nabla H\, dt$ are clearly visible.

As expected, the non-quadratic elastic potential energy requires higher-order quadrature of the corresponding forces to enforce sufficient precision in the case of elastic couplings.

5 | Perspective: Impedance Control

A simple control law, which one might want to implement using purely Cartesian positions and velocities, is impedance control in minimal coordinates (relative joint angles) [14]

$$\boldsymbol{\tau}^{\varphi}_{\text{imp}} = -(\boldsymbol{J}^{\varphi}_{\text{tcp}}(\boldsymbol{\varphi}))^{\top}(\boldsymbol{K}_x \tilde{\boldsymbol{x}}_{\text{tcp}} + \boldsymbol{D}_x \dot{\boldsymbol{x}}_{\text{tcp}}) + \nabla_{\varphi} V(\boldsymbol{\varphi}), \qquad (44)$$

where $\tilde{\boldsymbol{x}}_{\text{tcp}} \in \mathbb{R}^2$ is the TCP position error from a fixed reference, and $\boldsymbol{K}_x, \boldsymbol{D}_x > 0$ are desired symmetric Cartesian stiffness and damping matrices. A formulation in terms of the required control forces $\boldsymbol{F}_{\tau}$ to the COGs is

$$\boldsymbol{F}_{\tau,\text{imp}} = -\left(\boldsymbol{J}_{\text{tcp}}\boldsymbol{J}^{-1}\right)^{\top}(\boldsymbol{K}_x \tilde{\boldsymbol{x}}_{\text{tcp}} + \boldsymbol{D}_x \dot{\boldsymbol{x}}_{\text{tcp}}) + \nabla_x V(\boldsymbol{x}), \qquad (45)$$

with the constant TCP Jacobian according to (23). These forces must be realized by the joint torques $\boldsymbol{\tau}_{\text{imp}}$, and they must comply with the kinematic constraints, that is, there must exist suitable Lagrange multipliers $\boldsymbol{\lambda}_{\text{imp}}$ such that, see the first row of (2),

$$\boldsymbol{F}_{\tau,\text{imp}} = \begin{bmatrix} \boldsymbol{G}^{\top}(\boldsymbol{\xi}) & \boldsymbol{B}(\boldsymbol{\xi}) \end{bmatrix} \begin{bmatrix} \boldsymbol{\lambda}_{\text{imp}} \\ \boldsymbol{\tau}_{\text{imp}} \end{bmatrix} = \begin{bmatrix} \boldsymbol{G}^{\top}(\boldsymbol{\xi}) & \boldsymbol{B}_0(\boldsymbol{\xi}) \end{bmatrix} \begin{bmatrix} \boldsymbol{\lambda}_{\text{imp}} \\ \boldsymbol{L}^{-2}\boldsymbol{D}^{\top}\boldsymbol{\tau}_{\text{imp}} \end{bmatrix}. \qquad (46)$$

Writing

$$\begin{bmatrix} \boldsymbol{G}^{\top}(\boldsymbol{\xi}) & \boldsymbol{B}_0(\boldsymbol{\xi}) \end{bmatrix} = \begin{bmatrix} \boldsymbol{t}_1 \otimes \underbrace{\begin{bmatrix} \boldsymbol{\xi}_1 & \boldsymbol{\xi}_1^{\perp} \end{bmatrix}}_{=l_1^2 \boldsymbol{R}(\phi_1)} & \cdots & \boldsymbol{t}_N \otimes \underbrace{\begin{bmatrix} \boldsymbol{\xi}_N & \boldsymbol{\xi}_N^{\perp} \end{bmatrix}}_{=l_N^2 \boldsymbol{R}(\phi_N)} \end{bmatrix} \boldsymbol{P} = \boldsymbol{H}(\boldsymbol{\xi})\boldsymbol{P} \qquad (47)$$

with a permutation matrix $\boldsymbol{P} = \begin{bmatrix} \boldsymbol{e}_1 & \boldsymbol{e}_{N+1} & \cdots & \boldsymbol{e}_{N-1} & \boldsymbol{e}_{2N} \end{bmatrix}$, we recognize, comparing with (24), that

$$\boldsymbol{H}(\boldsymbol{\xi}) = \boldsymbol{J}^{-\top}\text{diag}\{l_1^2 \boldsymbol{R}(\phi_1), \ldots, l_N^2 \boldsymbol{R}(\phi_N)\}. \qquad (48)$$

With $\boldsymbol{R}(\phi_i)$ the absolute rotation matrices for all links, $\boldsymbol{H}(\boldsymbol{\xi})$ is always invertible. From (46), we therefore obtain the impedance control law, written completely in Cartesian link coordinates:

$$\boldsymbol{\tau}_{\text{imp}} = \boldsymbol{D}^{-\top}\text{diag}\{(\boldsymbol{\xi}_1^{\perp})^{\top}, \ldots, (\boldsymbol{\xi}_N^{\perp})^{\top}\}\boldsymbol{J}^{\top}\boldsymbol{F}_{\tau,\text{imp}}. \qquad (49)$$

6 | Conclusions

We discussed the modeling of planar serial kinematic chains with elastic couplings in terms of the *non-minimal* Cartesian coordinates and velocities of the link centers of gravity (COGs). The relative positions of the COGs with respect to the joints, expressed in the inertial frame, played the role of the absolute joint angles in a minimal setting. The corresponding forward kinematics mappings, their Jacobians, and their inverses were used to obtain the expressions for the total energy and the derived constraints and to cast the model in the form (2). The elongation of the parallel springs in a mono- and multi-articular setting was computed from vector chains based on the differences of the joint coordinates. The resulting elastic potential and its derivatives are non-polynomial. To ensure energy preservation in numerical integration with a mixed Galerkin scheme, sufficiently accurate quadrature of the corresponding integrals is required. In our simulations with a three-link model without and with elastic couplings, we recovered the expected results on exact constraint conservation, as well as the orders of the considered numerical schemes over the step size, which are determined by the quadrature rule for the energy gradient.

Analyzing the complementary structure of the derived constraint and the joint input matrices, their combination can be related to the absolute rotation matrices of the links, which are elements of the *special orthogonal group* SO(2). Their invertibility allows us to uniquely solve for Lagrange multipliers and joint torques if desired manipulator dynamics are prescribed in the fully actuated case, for example, via Cartesian impedance control. The impedance control law can then be written in terms of the link positions plus the TCP velocity, without trigonometric expressions of joint angles. Interesting application cases for this model-based control approach in non-minimal coordinates, which we are now extending to the 3D case, are control of manipulators based on only position measurements, as presented for example, in [15].

Data Availability Statement

The authors have nothing to report.

Endnotes

[1] See Subsection 3.3 for the expression of $\boldsymbol{M}$ in the planar N-link case.

[2] The sign of the second term is chosen to have an equal orientation of the constraint and input forces.

[3] $H(\boldsymbol{x}, \boldsymbol{p})|_{\boldsymbol{p}=\boldsymbol{M}\dot{\boldsymbol{x}}} = \boldsymbol{p}^{\top}\dot{\boldsymbol{x}} - L(\boldsymbol{x}, \dot{\boldsymbol{x}}) = \frac{1}{2}\dot{\boldsymbol{x}}^{\top}\boldsymbol{M}\dot{\boldsymbol{x}} + V(\boldsymbol{x})$

[4] Besides constrained mechanical systems, also distributed parameter systems, for example, from magneto-quasistatics or the Cahn–Hilliard equation, fit into this form, both on the continuous level and after Galerkin spatial discretization [7].

[5] If the COG is eccentric, replace α_i with the scaled rotation matrix $\boldsymbol{A}_i = \frac{L_i}{l_i}\boldsymbol{R}^{\top}(\beta_i)$.

[6] If not indicated otherwise, all expressions with index i are meant for $i = 1, \ldots, N$.

[7] In what follows, we will not distinguish between the formulations $\boldsymbol{G}(\boldsymbol{\xi})$ and $\boldsymbol{G}(\boldsymbol{x})$, also for other matrices.

[8] The vector $\boldsymbol{r}_{i+1}$ is a scaled version of $\boldsymbol{\xi}_{i+1}^{\perp}$ as defined in (30b).

References

1. R. M. Murray, S. S. Sastry, and L. Zexiang, *A Mathematical Introduction to Robotic Manipulation* (CRC Press, Inc., 1994).

2. T. Lee, M. Leok, and N. H. McClamroch, *Global Formulations of Lagrangian and Hamiltonian Dynamics on Manifolds*, vol. 13 (Springer, 2018).

3. M. Konz and J. Rudolph, "Redundant Configuration Coordinates and Nonholonomic Velocity Coordinates in Analytical Mechanics," *IFAC-PapersOnLine* 51, no. 2 (2018): 409–414.

4. M. Herrmann, D. Tiwari, P. Kotyczka, and R. Banavar, "Coordinate-Invariant Modeling and Control of a Three-DOF Robot Manipulator," *IFAC-PapersOnLine* 54, no. 19 (2021): 230–236.

5. M. Herrmann and P. Kotyczka, "Relative-Kinematic Formulation of Geometrically Exact Beam Dynamics Based on Lie Group Variational Integrators," *Computer Methods in Applied Mechanics and Engineering* 432 (2024): 117367.

6. P. Betsch and P. Steinmann, "Conservation Properties of a Time FE Method–Part III: Mechanical Systems with Holonomic Constraints," *International Journal for Numerical Methods in Engineering* 53, no. 10 (2002): 2271–2304.

7. H. Egger, O. Habrich, and V. Shashkov, "On the Energy Stable Approximation of Hamiltonian and Gradient Systems," *Computational Methods in Applied Mathematics* 21, no. 2 (2021): 335–349.

8. C. Kraus, M. Winckler, and H. G. Bock, "Modeling Mechanical DAE Using Natural Coordinates," *Mathematical and Computer Modelling of Dynamical Systems* 7, no. 2 (2001): 145–158.

9. J. G. de Jalón, "Twenty-Five Years of Natural Coordinates," *Multibody System Dynamics* 18, no. 1 (2007): 15–33.

10. P. Betsch, R. Siebert, and N. Sänger, "Natural Coordinates in the Optimal Control of Multibody Systems," *Journal of Computational and Nonlinear Dynamics* 7, no. 1 (2012).

11. J. Brüdigam, S. Sosnowski, Z. Manchester, and S. Hirche, "Variational Integrators and Graph-Based Solvers for Multibody Dynamics in Maximal Coordinates," *Multibody System Dynamics* 61, no. 3 (2024): 381–414.

12. C. W. Gear, B. Leimkuhler, and G. K. Gupta, "Automatic Integration of Euler-Lagrange Equations With Constraints," *Journal of Computational and Applied Mathematics* 12 (1985): 77–90.

13. A. Müller, "Screw and Lie Group Theory in Multibody Kinematics," *Multibody System Dynamics* 43, no. 1 (2018): 37–70.

14. N. Hogan, "Impedance Control: An Approach to Manipulation: Part II—Implementation," *Journal of Dynamic Systems, Measurement, and Control* 107, no. 1 (1985): 8–16.

15. A. P. R. Lauer, O. Lerke, B. Blagojevic, V. Schwieger, and O. Sawodny, "Tool Center Point Control of a Large-Scale Manipulator Using Absolute Position Feedback," *Control Engineering Practice* 131 (2023): 105388.